Thermal conductivity of non-stoichiometric americium oxide: A molecular dynamics study

Teppei Uchida [a,b], Tatsumi Arima [a,*], Kazuya Idemitsu [a], Yaohiro Inagaki [a]

[a] Department of Applied Quantum Physics and Nuclear Engineering, Faculty of Engineering, Kyushu University, 744 Motooka, Fukuoka 819-0395, Japan
[b] Nuclear Fuel Cycle Engineering Laboratories, Japan Atomic Energy Agency, 4-33, Muramatsu, Tokai-mura, Naka-gun, Ibaraki 319-1194, Japan

ARTICLE INFO

ABSTRACT

The aim of this paper is to investigate the influence of multi-valency of americium in its oxide for the lowering of the thermal conductivity and the uncertainty in measurement. In the present study, thermal conductivity of non-stoichiometric americium oxide was evaluated up to 2000 K by the non-equilibrium molecular dynamics calculations using the Born–Mayer–Huggins interatomic potential with the partially ionic model. The oxygen-to-americium ratio (O/Am) was varied from 1.6 to 1.9, which corresponded to the variation of the ratio of Am^{3+}/Am^{4+}. So, we prepared potential parameters for both Am^{3+} and Am^{4+}. The calculated thermal conductivity of non-stoichiometric americium oxide decreased with an increase of temperature, and the degree of the temperature dependence became smaller with a decrease of the O/Am ratio. This was mainly caused by the phonon-scattering due to oxygen vacancies induced with Am^{3+} ions. Comparing two supercells in which (1) short-range ordered Am^{3+} clusters were contained and (2) Am^{3+} ions were randomly distributed, the thermal conductivity of the former seemed to be somewhat larger than that of the latter.

© 2010 Elsevier B.V. All rights reserved.

1. Introduction

For a nuclear fuel cycle, minor actinides (MA: Np, Am, Cm) are the key elements because these are possible to be used as MOX containing MA, or disposed a transuranic waste. In a novel concept for the nuclear transmutation system, these MA might be used as a target fuel, e.g. CERCER (ceramic–ceramic) or CERMET (ceramic–metal) fuel. Especially, americium isotopes have the high and lasting radiotoxicity. In addition, an americium ion shows the multi-valency in the oxide form from the view of a chemical property [1]. For high temperatures like a fuel operating temperature, the oxidation state of the americium ion is sensitive to oxygen partial pressure. As a result, the americium oxide often forms to be the mixture of dioxide and sesquioxide. Therefore, there were sometimes discrepancies among the empirical, semi-empirical and theoretical assessments [2–11]. For example, the literature data of the thermal conductivity of americium dioxide varied from ca. 3 to 9 W m^{-1} K^{-1} around 300 K [3,9,10].

We have evaluated various thermal properties of actinide oxides, e.g. uranium oxides and plutonium oxides and their solid solution by the molecular dynamics (MD) simulation so far [12–14]. Recently, thermal properties of stoichiometric AmO_2 and Am_2O_3 have been reported [15]. And also, other researchers have demonstrated the validity of MD simulation for the analyses of thermal

properties such as thermal expansion, heat capacity, thermal conductivity and so on [10,12,13]. Especially for the thermal conductivity, we have developed non-equilibrium MD (NEMD) method as the alternative simulation technique for equilibrium MD (EMD) method and have evaluated the effect of oxygen non-stoichiometry in oxide fuels [14]. In the present study, we therefore performed NEMD simulations for non-stoichiometric americium oxide AmO_{2-x} ($x < 0.5$) in order to systematically investigate thermal conductivities.

2. Molecular dynamics simulation

2.1. Interatomic potential function and non-equilibrium molecular dynamics simulation

In the present study, the MXDORTO program customized for the calculation of the thermal conductivity in non-equilibrium system was used in the MD simulation, and the original code was developed by Hirao and Kawamura [16]. Here, we employed the Born–Mayer–Huggins (BMH) interatomic potential with the partially ionic model (PIM) to each ion pair in crystals. The interatomic potential function consists of three terms of Coulomb interaction, repulsive short-range interaction and van der Waals interaction.

$$U_{PIM}(r_{ij}) = \frac{z_i z_j e^2}{r_{ij}} + f_0(b_i + b_j)\exp\left(\frac{a_i + a_j - r_{ij}}{b_i + b_j}\right) - \frac{c_i c_j}{r_{ij}^6}, \quad (1)$$

* Corresponding author. Tel./fax: +81 92 802 3494.
E-mail address: arima@nucl.kyushu-u.ac.jp (T. Arima).

where f_0 (=6.9511×10^{-11} N) is an adjustable parameter. Potential parameters, a_i, b_i and c_i, are associated with an ion of type i. In Eq. (1), z_i is the effective charge of a type i ion, and an ionic bonding of 67.5% is assumed for each ion in the present simulated system [12–15,17,18]. In order to calculate the thermal conductivity of non-stoichiometric americium oxide, we needed the potential parameters for both Am^{4+}–O^{2-} and Am^{3+}–O^{2-} systems. In the previous study [15], these potential parameters were determined to reproduce lattice structures, thermal expansions and bulk moduli experimentally obtained for fluorite AmO$_2$ and cubic bixbyite Am$_2$O$_3$ crystals [1,2,5–7,19–21]. Potential parameters summarized in Table 1 were adequate for AmO$_2$, however these gave a little small bulk modulus of Am$_2$O$_3$.

As one of the alternatives to the EMD method, the homogeneous NEMD one proposed by Evans and Morriss [22] was applied to calculate the thermal conductivity in the present study. It gave the small errors of the thermal conductivities than the EMD at low temperatures. Errors in the EMD calculations were originated from the large fluctuation of the auto-correlation function of the heat fluxes [15]. As described below, the NEMD method can be kept away from such a drawback. In the homogeneous NEMD scheme, dynamics of the particles in the simulated cell are governed by the following equations of motion:

$$\frac{d\vec{q}_i}{dt} = v_i, \tag{2}$$

$$\frac{d\vec{p}_i}{dt} = \vec{F}_i + \overset{\leftrightarrow}{D}_i \vec{F}_{ext}(t), \tag{3}$$

where $\vec{q}_i$ and $\vec{p}_i$ are the generalized coordinate and momentum of ith particle, v_i the velocity, $\vec{F}_i$ the force, $\vec{F}_{ext}$ the perturbed external force field parameter coupled with $\overset{\leftrightarrow}{D}_i$ the tensor parameter. Here, $\overset{\leftrightarrow}{D}_i$ means the deviation energy of ith particle from average of energy in the N-particle system [23]. For $\vec{F}_{ext} = (F_{ext}, 0, 0)$, the thermal conductivity in x direction is written by

$$\kappa = \lim_{F_{ext} \to 0} \lim_{t \to \infty} \frac{\left\langle \vec{j}_E(t) \right\rangle}{V T F_{ext}}. \tag{4}$$

Table 1
Potential parameters of the Am–O system.

Ion	z_i	a_i (nm)	b_i (nm)	c_i ($J^{0.5}$ nm^3 mol$^{-0.5}$)	Reference
Am^{4+}	2.7	0.1282	0.00373	0.0	[15]
Am^{3+}	2.025	0.1271	0.00301	0.0	[15]
O^{2-}	−1.35	0.1847	0.01660	1.294	[17,18]

Therefore, in the NEMD scheme, the thermal conductivity is defined as the proportional constant between the time-averaged energy current (heat flux) and the perturbed external force field parameter. In the above equations, $\vec{j}_E(t)$ is generally written by

$$\vec{j}_E(t) = \sum_{i=1}^{N} \left[\frac{m_i v_i^2}{2} + \frac{1}{2} \sum_{j \neq i} U(r_{ij}) \right] \vec{v}_i + \frac{1}{2} \sum_{i=1}^{N} \vec{v}_i \cdot \vec{r}_{ij} \vec{F}_{ij}. \tag{5}$$

The energy current in the Coulomb system for the present study was given by Bernu and Vieillefosse [24]. In the EMD, the calculation of the auto-correlation functions of energy currents expressed in Eq. (5) was required, but not required in the NEMD [15].

2.2. Supercells and simulation procedure

In the present study, we prepared two types of supercells for AmO$_{2-x}$ crystal. One is the supercell contains the short-range ordered cation clusters, which are tetrahedrons consisting of Am^{3+}. Hereafter, this supercell is called SC1 and is shown in Fig. 1a. For the initial configuration of the SC1 supercell, 1/8 unit cell of bixbyite Am$_2$O$_3$ (Am^{3+} ions: 4, O^{2-}: 6) and a unit cell of fluorite AmO$_2$ (Am^{4+} ions: 4, O^{2-}: 8) were mixed for the specified O/Am ratio because the lattice constant of bixbyite is about twice as large as that of fluorite. Thus, cubic SC1 supercell consisted of less than 1500 ions but number of cations was strictly 500. The other is one in which Am^{3+} ions were randomly substituted for Am^{4+} ions on cation sub-lattice sites of $5 \times 5 \times 5$ fluorite unit cells, which means the positions of Am^{3+} ions were given by random numbers generated by a computer. Subsequently, O^{2-} ions were removed in accordance with the amount of Am^{3+} ions. This supercell is called SC2 and is shown in Fig. 1b. According to the phase diagram of Am–O system, in the O/Am range between 1.6 and 1.9, fluorite AmO$_{2-x}$ dominates above roughly 1100 K, however bixbyite Am$_2$O$_{3+y}$ and fluorite AmO$_{2-x}$ coexists at low temperatures [25]. Unfortunately, experimental results are rather restricted for studies of the phase diagram. Of course, the configurations of lattice defects are not understood sufficiently for this system. Therefore, although two types of supercell described above might not reflect the defect configuration actually formed in the real crystal, we made such an assumption, i.e. SC1 and SC2.

The homogeneous NEMD calculation was performed under the periodic boundary conditions, and temperature of the system was controlled with the Nóse thermostat. The thermostat mass was 1×10^{-13} kg m^2 [16]. Following the initial relaxation calculation with 2×10^4 steps (=40 ps), the NEMD simulation was performed
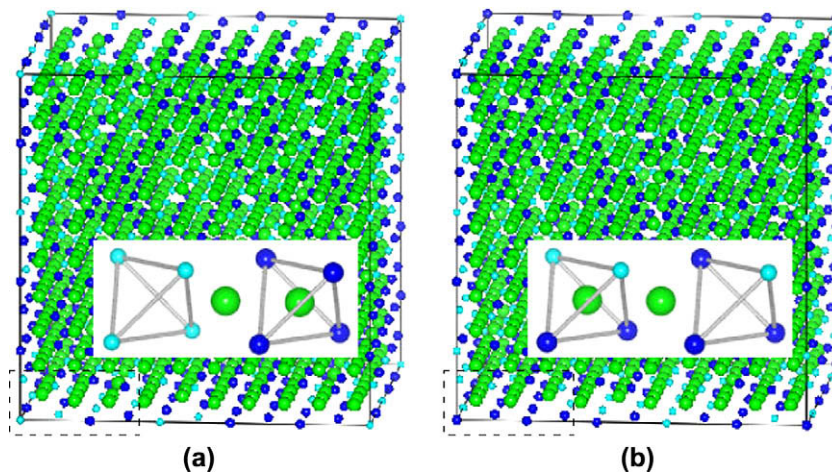

Fig. 1. Simulated supercells in which (a) tetrahedron consisting of Am^{3+} contained (SC1) and (b) Am^{3+} randomly distributed (SC2). Large green ball stands for O^{2-}, small blue one Am^{4+} and light blue one Am^{3+}. Each enlarged image of defect configuration is also shown here. (For interpretation of the references to colour in this figure legend, the reader is referred to the web version of this article.)

for 5×10^4 steps (=100 ps) in the *NVT* ensemble for 5 or 6 different F_{ext} values and directions of x, y and z. During the calculation, the supercell shape was kept to cubic even for the system including oxygen vacancies.

3. Results and discussion

Fig. 2 shows the O/Am dependence of lattice constant of AmO_{2-x} around 300 K. In this figure, the experimental result and Vegard's law, which is predicted by a mixture of bixbyite and fluorite, are plotted, together with the results obtained from NEMD cal-culations. The experimental result by Chikalla clearly shows the coexistence of hyperstoichiometric bixbyite and stoichiometric fluorite [25]. Our calculated results are in good agreement with experimental one and Vegard's law, and the lattice constants of SC1 and SC2 increase with a decrease of O/Am ratio, which is that the substitution of Am^{3+} with inducing oxygen vacancies results in an increase of the lattice constant. The difference in lattice constant between SC1 and SC2 are rather small. Such a tendency was caused from an expansion of the distance between nearest-neighbor (NN) oxygen ions. The pair correlation function of O–O shows in Fig. 3. Although the difference between SC1 and SC2 cannot be observed, NN distance apparently increases with decreasing O/Am ratio.
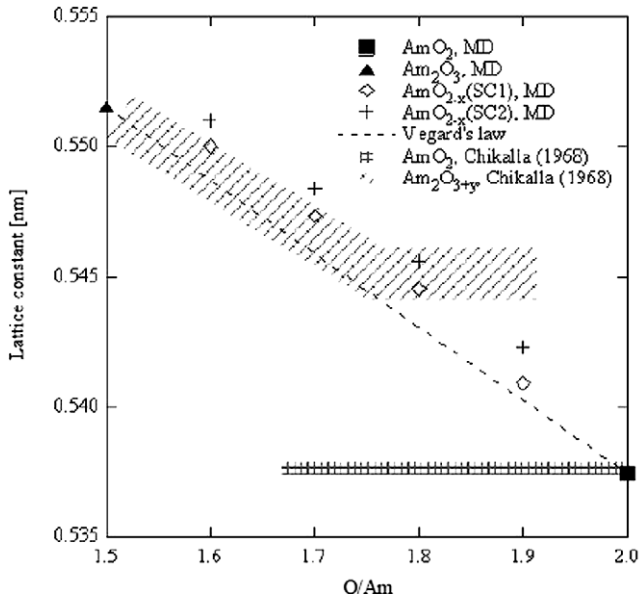

Fig. 2. Lattice constants of AmO_{2-x} as a function of the O/Am ratio around 300 K.
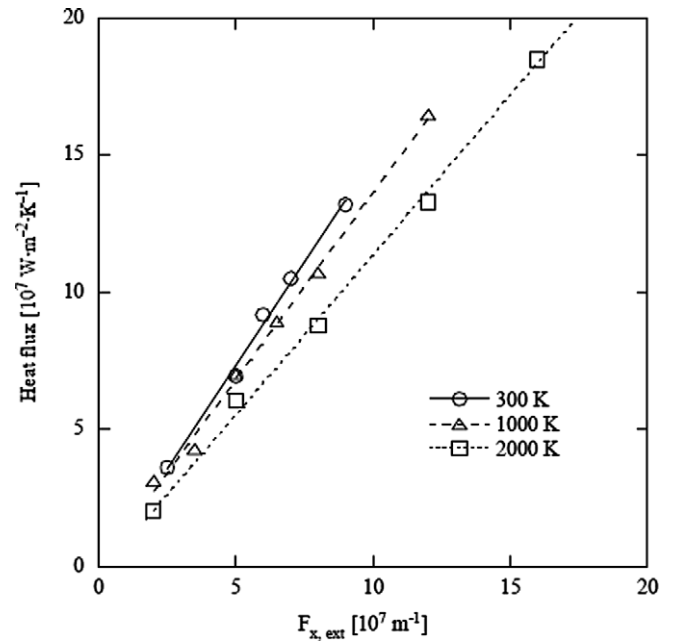

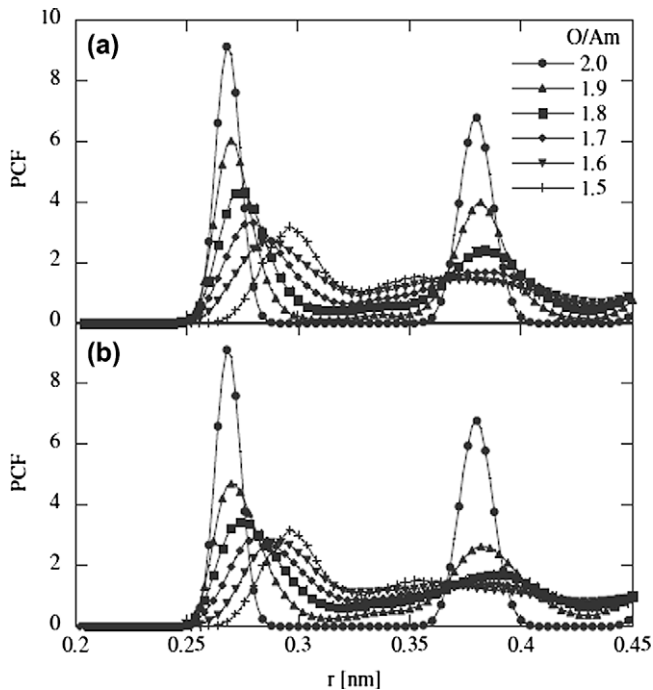**Fig. 4.** Heat flux of $AmO_{1.8}$ as a function of perturbed external force field.

Fig. 3. Pair correlation function (PCF) of O–O ions as a function of distance for (a) SC1 and (b) SC2 supercells.
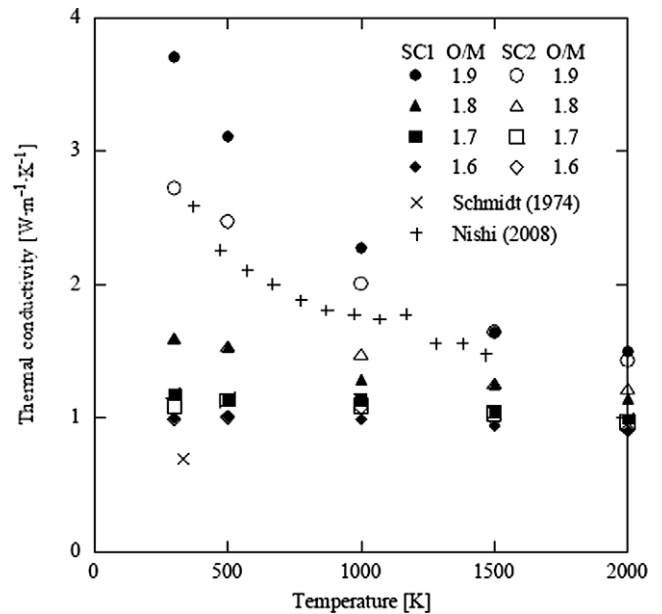

Fig. 5. Thermal conductivity obtained from NEMD calculation for AmO_{2-x} as a function of temperature.

The thermal conductivities of non-stoichiometric oxides were evaluated by NEMD calculations. The calculated thermal conductivity was determined by Eq. (4). For $AmO_{1.8}$, the relationship between the time-averaged heat flux and the perturbed external force field parameter is shown in Fig. 4. The value of the heat flux increases with respect to F_{ext}, which means the linear response between the heat flux and F_{ext}. When too large F_{ext} was applied to the system, the linear response broke down. The slope of the linear relation observed decreases with an increase of temperature because of phonon–phonon interaction (Umklapp process) at high temperatures.

In the previous study, we reported that the calculated thermal conductivity of AmO_2 was comparable with that of UO_2 [26] and was inversely proportional to temperature, whereas that of Am_2O_3 was ca. 0.8 W m^{-1} K^{-1} regardless of temperature [15]. The calculated thermal conductivities of AmO_{2-x} are shown in Fig. 5, together with the literature data. The low thermal conductivity less than 1.0 W m^{-1} K^{-1} was measured for AmO_{2-x} by Schmidt, where oxygen deficiency x was unclear [8]. Recently, the temperature dependence of thermal conductivity of AmO_{2-x} was reported by Nishi et al. [3]. The reported O/Am ratio varied from 1.73 to 1.90. The MD calculation seems to be comparable with experimental
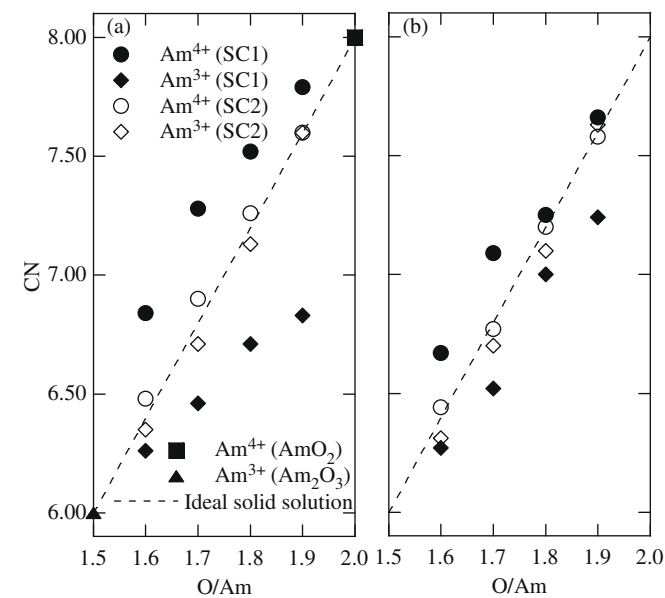
data measured by Nishi et al. [3], and predicts that the O/Am ratio is near 1.5 for Schmidt's experiment [8]. At the O/Am ratio of 1.9, the calculated thermal conductivity clearly decreases with an increase of temperature for both SC1 and SC2. With decreasing the O/Am ratio, the thermal conductivity decreases, and the degree of the temperature dependence also decreases, which means that at high O/Am ratios, both Umklapp process and phonon-defect interaction contribute to the lowering of thermal conductivity, whereas at low O/Am ratios, the phonon-defect interaction dominates. Furthermore, from the point of view of the defect configuration, the thermal conductivity of SC1 is higher than that of SC2 for the O/Am = 1.9 at low temperatures but is almost same for small O/Am ratios. Fig. 6 shows the oxygen coordination number (CN) of Am^{3+} or Am^{4+} ion, which figures out the local defect configuration around a cation. At 300 K, the initial configuration still remains even after the relaxation calculation because oxygen cannot move around in the supercell (Fig. 6a). As a result, the difference in CN for SC1 can be clearly observed between Am^{3+} and Am^{4+}. On the other hand, such a difference cannot be observed for SC2, and CN is almost same as one given by ideal solid solution, i.e. random distributions of Am^{3+} ions and oxygen vacancies. At 2000 K (Fig. 6b), the difference in CN between SC1 and SC2 becomes small because oxygen can easily move around. However, the defect configuration of SC1 still remains at 2000 K. Therefore, although a local configuration of defects is different between SC1 and SC2, the thermal conductivity is almost same for the O/Am $\leqslant$ 1.8 at even low temperatures. It seems that the oxygen deficiency, x, simply effects the thermal conductivity of AmO_{2-x}, where $x \geqslant 0.2$. Here, oxygen vacancy and Am^{3+} ion, both contribute to oxygen deficiency. Although the interatomic potential function is different between Am^{4+} and Am^{3+} ions, both ions occupy the cation sub-lattice sites and cause little alteration of its lattice structure. On the other hand, oxygen vacancies cause the significant alteration of anion sub-lattice structure. Therefore, it is highly possible that oxygen vacancies more contribute to the lowering of thermal conductivity than Am^{3+} ions if the phonon dispersion of AmO_2 is almost kept even for the system where some defects are introduced, i.e. AmO_{2-x}. The following discussion is also based on this hypothesis.

In general, the thermal conductivity can be expressed in $(A + B \cdot T)^{-1}$, where A and B are constants, T is temperature. A is the thermal resistance caused by the phonon-defect interaction while $B \cdot T$ is one caused by the phonon–phonon interaction. The values of A and B, which are estimated from thermal conductivities in Fig. 5, are plotted as a function of the O/Am ratio in Fig. 7a and b, respectively. Our calculated results show that A of stoichiometric AmO_2 is almost zero and increases with a decrease of the O/Am ratio, which is interpreted that oxygen deficiency strongly effects the lowering of thermal conductivity at the wide range of the O/Am
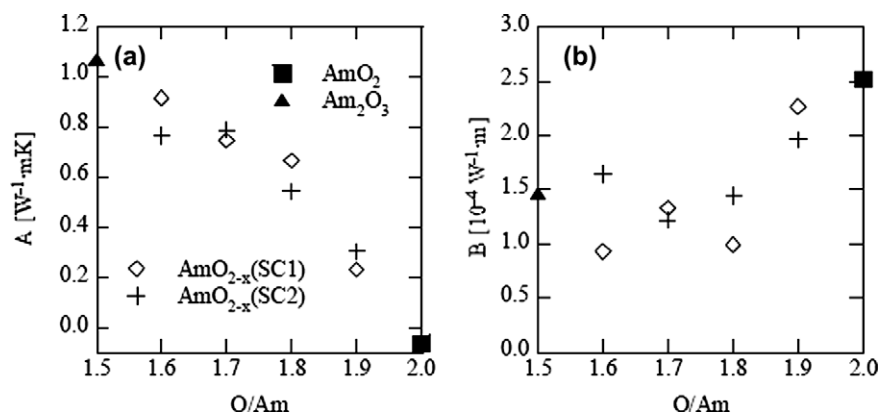

Fig. 6. Oxygen coordination number (CN) as a function of O/Am ratio for (a) 300 K and (b) 2000 K.

Fig. 7. A (a) and B (b) constants as a function of O/Am ratio. Here, the temperature dependence of thermal conductivity is given by $(A + B \cdot T)^{-1}$.

ratio. These results mean that the thermal conductivity of stoichiometric AmO_2 well obeys the above thermal resistance model. Furthermore, the thermal resistance A of cubic Am_2O_3 is not zero, which means that if the lattice structure of AmO_2 is ideal fluorite, that of Am_2O_3 is considered to be deformed fluorite or fluorite including defects. It is because the crystal structure of Am_2O_3 is bixbyite and positions of Am and O ions except for oxygen vacancies in Am_2O_3 are almost same as those of fluorite AmO_2. On the other hand, B values for O/Am = 1.9 are comparable with that of AmO_2, whereas at O/Am $\leqslant$ 1.8, these values are almost same as that of Am_2O_3. Hence, in the Am–O system, the temperature dependence of thermal conductivity is rapidly decreased with an increase of oxygen deficiency, and as a result, the thermal conductivity of AmO_{2-x} approaches to that of Am_2O_3.

4. Conclusions

In the present study, the thermal conductivity of AmO_{2-x} was evaluated by NEMD simulation using the BMH potential function with the PIM. The thermal conductivity was obtained as the proportional constant between the energy current and the perturbed external force field parameter in the homogeneous NEMD system. The calculated results were almost comparable with experimental results obtained from AmO_{2-x}. Considering the O/Am ratio dependence, the thermal conductivity calculated from NEMD simulation decreases with an increase of temperature at O/Am $\geqslant$ 1.9 and almost constant with respect to temperature at O/Am $\leqslant$ 1.8, which means that both phonon–phonon and phonon–defect interactions contributes to the lowering of thermal conductivity at high O/Am ratios and the phonon–defect interaction dominates it at low O/Am ratios. From the point of view of defect configurations, under the condition of O/Am = 1.9 and low temperatures, SC1 supercell with Am^{3+} tetrahedron clusters has higher thermal conductivity than SC2 supercell in which Am^{3+} and oxygen vacancies were randomly distributed. For other conditions, almost comparable results were obtained for SC1 and SC2 supercells. This is the reason why the partially coherent phonon propagates in crystal for the former condition since the local defect configuration still remains, whereas the phonon propagation is strongly disturbed by defects, i.e. oxygen vacancies, under the latter condition.

References

[1] E.H.P. Cordfunke, R.J.M. Konings, Thermochemical Data for Reactor Materials and Fission Products, North-Holland, Amsterdam, 1990.
[2] J.A. Fahey, Inorg. Nucl. Chem. Lett. 20 (1974) 459.
[3] T. Nishi, M. Takano, A. Itoh, M. Akabori, Y. Arai, K. Minato, M. Numata, J. Nucl. Mater. 373 (2008) 295.
[4] K. Minato, M. Takano, T. Nishi, A. Itoh, M. Akabori, Recent Adv. Actinide Sci. (2006) 317.
[5] J.P. Dancausse, E. Gering, S. Heathman, U. Benedict, J. Nucl. Sci. Technol. 3 (Suppl.) (2002) 136.
[6] S. Li, R. Ahuja, B. Johansson, High Press. Res. 22 (2002) 471.
[7] M. Idiri, T.L. Bihan, S. Heathman, J. Rebizant, Phys. Rev. B 70 (2004) 14113.
[8] H.E. Schmidt, in: Proc. 4ième Journées d'Actinides, Harwell, UK, 1974, Atomic Energy Research Establishment Report AERE-R-7961, 1975.
[9] K. Bakker, R.J.M. Konings, J. Nucl. Mater. 254 (1998) 129.
[10] S.E. Lemehov, V. Sobolev, P. Van Uffelen, J. Nucl. Mater. 320 (2003) 66.
[11] K. Kurosaki, M. Imamura, I. Sato, T. Namekawa, M. Uno, S. Yamanaka, J. Nucl. Sci. Technol. 41 (2004) 827.
[12] T. Arima, S. Yamasaki, Y. Inagaki, K. Idemitsu, J. Alloys Compd. 400 (2005) 43.
[13] T. Arima, S. Yamasaki, Y. Inagaki, K. Idemitsu, J. Alloys Compd. 415 (2006) 43.
[14] T. Arima, S. Yamasaki, K. Idemitsu, Y. Inagaki, J. Nucl. Mater. 376 (2008) 139.
[15] T. Uchida, T. Arima, K. Idemitsu, Y. Inagaki, Comput. Mater. Sci. 45 (2009) 229.
[16] K. Hirao, K. Kawamura, Material Design using Personal Computer, Shokabo, Tokyo, 1994.
[17] H. Inaba, R. Sagawa, H. Hayashi, K. Kawamura, Solid State Ionics 122 (1999) 95.
[18] H. Hayashi, R. Sagawa, H. Inaba, K. Kawamura, Solid State Ionics 131 (2000) 281.
[19] C. Thiriet, R.J.M. Konings, J. Nucl. Mater. 320 (2003) 292.
[20] D. Taylor, Br. Ceram. Trans. J. 83 (1984) 92.
[21] R.D. Shannon, Acta Crystallogr. A32 (1976) 751.
[22] D.J. Evans, G.P. Morriss, Statistical Mechanics of Nonequilibrium Liquids, Academic, London, 1990.
[23] S. Motoyama, Y. Ichikawa, Y. Hiwatari, A. Oe, Phys. Rev. B 60 (1999) 292.
[24] B. Bernu, P. Vieillefosse, Phys. Rev. A 18 (1978) 2345.
[25] T.D. Chikalla, L. Eyring, J. Inorg. Nucl. Chem. 30 (1968) 133.
[26] S. Fukushima, T. Ohmichi, A. Maeda, M. Honda, J. Nucl. Mater. 115 (1983) 118.